

# Complex Saddle Points and Disorder Lines in QCD at finite temperature and density

Hiromichi Nishimura

*Faculty of Physics, University of Bielefeld, D-33615 Bielefeld, Germany*

Michael C. Ogilvie and Kamal Pangaeni

*Department of Physics, Washington University, St. Louis, MO 63130 USA*

(Dated: 11/17/14)

## Abstract

The properties and consequences of complex saddle points are explored in phenomenological models of QCD at non-zero temperature and density. Such saddle points are a consequence of the sign problem, and should be considered in both theoretical calculations and lattice simulations. Although saddle points in finite-density QCD are typically in the complex plane, they are constrained by a symmetry that simplifies analysis. We model the effective potential for Polyakov loops using two different potential terms for confinement effects, and consider three different cases for quarks: very heavy quarks, massless quarks without modeling of chiral symmetry breaking effects, and light quarks with both deconfinement and chiral symmetry restoration effects included in a pair of PNJL models. In all cases, we find that a single dominant complex saddle point is required for a consistent description of the model. This saddle point is generally not far from the real axis; the most easily noticed effect is a difference between the Polyakov loop expectation values  $\langle \text{Tr}_F P \rangle$  and  $\langle \text{Tr}_F P^\dagger \rangle$ , and that is confined to small region in the  $\mu - T$  plane. In all but one case, a disorder line is found in the region of critical and/or crossover behavior. The disorder line marks the boundary between exponential decay and sinusoidally modulated exponential decay of correlation functions. Disorder line effects are potentially observable in both simulation and experiment. Precision simulations of QCD in the  $\mu - T$  plane have the potential to clearly discriminate between different models of confinement.

## I. INTRODUCTION

The phase structure of QCD at finite density and temperature is of fundamental importance, and can be studied experimentally, theoretically and via lattice simulations. Nevertheless, progress has been slow, in part because of the sign problem, which afflicts both phenomenological models and lattice simulations. The sign problem is found in many area of physics [1–3]. In QCD, the quark contribution to the partition function, given as a functional determinant dependent on the gauge field, is complex for typical gauge field configurations when the quark chemical potential  $\mu$  is non-zero. It is natural to consider the analytically continuation of the gauge field into the complex plane. Some progress has been made in incorporating this idea into lattice simulations [4–10]. Here we show that the consideration of complex saddle points provides a conceptually cohesive phenomenological model of QCD at finite  $T$  and  $\mu$ . Our results can provide guidance for lattice simulations by indicating the behavior of the dominant field configuration, within a phenomenological framework. We will show that certain features of the saddle point appear to be independent of the choice of a particular phenomenological model. Moreover, we will identify a new property of QCD at finite density, the occurrence of a disorder line, that may have observable consequences in experiment and/or lattice simulation. Some feature associated with the disorder line differentiate strongly between different phenomenological models, and may thus have an impact on our understanding of confinement.

The remainder of this paper is organized as follows. In section II, we provide a simple example based on the the  $U(1)$  group that indicates the need for complex saddle points. Section III reviews the formalism first developed in our previous work [11]. We pay particular attention to the existence and consequences of an antilinear symmetry  $\mathcal{CK}$  in finite density field theories, where  $\mathcal{C}$  is charge conjugation and  $\mathcal{K}$  is complex conjugation; in some sense this symmetry replaces charge conjugation symmetry when  $\mu \neq 0$ . The following section, section IV, describes the different phenomenological models we study using an effective potential for the Polyakov loop  $P$  and chiral condensate  $\bar{\psi}\psi$ . We do not consider other possible condensates in this work, such as the color superconducting condensate, deferring this to later work. A total of six different models are considered. We use two different models for the confining part of the effective potential, Model A and Model B, taken from [12]. We consider three cases of quarks, always with two flavors: heavy quarks, massless quarks with

no chiral dynamics and a full treatment of light quarks, with chiral dynamics included via a bosonized four-fermion interaction. Our most realistic models are therefore of Polyakov-Nambu-Jona Lasinio (PNJL) type, with the major new feature the consideration of complex saddle points of the effective potential. Section V, VI and VII describe in detail the results for the three different cases of quarks. A final section offers conclusions.

## II. SIMPLE U(1) EXAMPLE

As an illustration of the role of analytic continuation in field space for models with non-zero chemical potential, we consider a single-site model, where a particle propagates in a closed loop in Euclidean time, always returning to the same lattice site. The model has a hopping parameter  $J$ , a dimensionless chemical potential  $\mu$  and a  $U(1)$  background field  $\theta$  [13]. The partition function is

$$Z = \int \frac{d\theta}{2\pi} e^S \quad (1)$$

where

$$S = J [e^{\mu+i\theta} + e^{-\mu-i\theta}]. \quad (2)$$

The action  $S$  is complex, so  $Z$  has a sign problem. It is easy to find  $Z$  exactly by a strong-coupling expansion in  $J$ :

$$Z = \sum_{n=0}^{\infty} \frac{J^{2n}}{(n!)^2} = I_0(J), \quad (3)$$

where  $I_0(J)$  is the modified Bessel function of order 0. Similar results can be obtained for expectation values such as  $\langle e^{i\theta} \rangle$ , which are zero-dimensional analogs of Polyakov loops. It is instructive to consider  $Z$  as a contour integral in the variable  $z = \exp(i\theta)$ :

$$Z = \int_{|z|=1} \frac{dz}{2\pi iz} \exp [Jze^{\mu} + Jz^{-1}e^{-\mu}]. \quad (4)$$

We ask if the contour  $|z| = 1$  can be deformed to a contour  $C$  along which  $S$  is real. The contour  $C$  is given by the circle  $|z| = e^{-\mu}$ . Making a change of variable  $\theta \rightarrow \theta + i\mu$ , we recover exact results such as

$$\begin{aligned} Z &= I_0(J) \\ \langle e^{i\theta} \rangle &= e^{-\mu} \frac{I_1(J)}{I_0(J)} \\ \langle e^{-i\theta} \rangle &= e^{+\mu} \frac{I_1(J)}{I_0(J)}. \end{aligned} \quad (5)$$

We apply a saddle-point method to the original integral, looking for the saddle-point in the complex plane. The saddle point satisfies

$$e^\mu - e^{-\mu}/z^2 = 0 \quad (6)$$

so the saddle is at  $i\theta = -\mu$ . Returning to the original notation, we approximate  $Z$  by

$$Z \approx \int \frac{d\theta}{2\pi} \exp \left[ 2J - \frac{1}{2} 2J\theta^2 \right] = \frac{e^{2J}}{\sqrt{4\pi J}} \quad (7)$$

which is the leading-order asymptotic behavior of  $I_0(2J)$ . A similar evaluation for the expectation values yields

$$\begin{aligned} \langle e^{i\theta} \rangle &\simeq e^{-\mu} \\ \langle e^{-i\theta} \rangle &\simeq e^{+\mu}. \end{aligned} \quad (8)$$

If we had used  $Re(S) = J(e^\mu + e^{-\mu}) \cos \theta$  as a starting point for a steepest descents calculation, the result for  $Z$  would have been

$$\frac{e^{J(e^\mu + e^{-\mu})}}{\sqrt{2\pi J(e^\mu + e^{-\mu})}} \quad (9)$$

which does not represent the correct asymptotic behavior.

It is important to emphasize that neither a deformation of the contour into the complex plane nor the use of complex saddle points is required in an exact evaluation of  $Z$  and related quantities. However, many methods, from perturbation theory to importance sampling in lattice simulations, rely implicitly or explicitly on the existence of appropriate saddle points. In this simple  $U(1)$  model, the use of complex saddle points naturally allows the expected values of the Polyakov loops for particle and antiparticles to be different:  $\langle e^{i\theta} \rangle \neq \langle e^{-i\theta} \rangle$ . In an exact calculation using a real contour for  $\theta$ , this result must be recovered from rapid fluctuations in the integration. A saddle point approximation incorrectly using  $Re(S)$  for the location of saddle points would have obtained  $\langle e^{i\theta} \rangle = \langle e^{-i\theta} \rangle$  at leading order.

### III. FORMALISM FOR $SU(N)$ GAUGE THEORIES AT FINITE DENSITY

We now consider an  $SU(N)$  gauge theory coupled to fermions in the fundamental representation. It is well-known that the Euclidean Dirac operator has complex eigenvalues when

a non-zero chemical potential is introduced [1]. This can be understood as an explicit breaking of charge conjugation symmetry  $\mathcal{C}$ . The log of the fermion determinant,  $\log \det(\mu, A)$ , which is a function of the quark chemical potential  $\mu$  and the gauge field  $A$ , can be formally expanded as a sum over Wilson loops with real coefficients. For a gauge theory at finite temperature, the sum includes Wilson loops that wind non-trivially around the Euclidean timelike direction; Polyakov loops, also known as Wilson lines, are examples of such loops. At  $\mu = 0$ , every Wilson loop  $\text{Tr}_F W$  appearing in the expression for the fermion determinant is combined with its conjugate  $\text{Tr}_F W^\dagger$  to give a real contribution to path integral weighting. More formally, charge conjugation acts on matrix-valued Hermitian gauge fields as

$$\mathcal{C} : A_\mu \rightarrow -A_\mu^t \quad (10)$$

where the overall minus sign is familiar from QED, and the transpose interchanges particle and antiparticle, *e.g.*,  $W^+$  and  $W^-$  in  $SU(2)$ . This transformation law in turn implies that  $\mathcal{C}$  exchanges  $\text{Tr}_F W$  and  $\text{Tr}_F W^\dagger$  so unbroken charge symmetry implies a real fermion determinant. When  $\mu \neq 0$ , Wilson loops with non-trivial winding number  $n$  in the  $x_4$  direction receive a weight  $e^{n\beta\mu}$  while the conjugate loop is weighted by  $e^{-n\beta\mu}$  and invariance under  $\mathcal{C}$  is explicitly broken. However, there is a related antilinear symmetry which is unbroken:  $\text{Tr}_F W$  transforms into itself under the combined action of  $\mathcal{CK}$ , where  $\mathcal{K}$  is the fundamental antilinear operation of complex conjugation. Thus the theory is invariant under  $\mathcal{CK}$  even in the case  $\mu \neq 0$ . This symmetry is an example of a generalized  $\mathcal{PT}$  (parity-time) symmetry transformation [14, 15]; theories with such symmetries form special class among theories with sign problems. For fermions,  $\mathcal{CK}$  symmetry implies the well-known relation  $\det(-\mu, A_\mu) = \det(\mu, A_\mu)^*$  for Hermitian  $A_\mu$ , a relation which is often derived using a  $\gamma_5$  transformation of the Dirac operator. The advantage of using  $\mathcal{CK}$  is that it is more general, leading to more insight into the sign problem and applying to bosons as well as to fermions. For example, it is easy to see that our simple zero-dimensional  $U(1)$  model in the preceding section is invariant under the combined action of  $\mathcal{K} : i \rightarrow -i$  and  $\mathcal{C} : \theta \rightarrow -\theta$ .

For phenomenological models, the existence of  $\mathcal{CK}$  symmetry leads naturally to the consideration of complex but  $\mathcal{CK}$ -symmetric saddle points.  $\mathcal{CK}$  symmetry will map any saddle-point configuration  $A_\mu^{(1)}$  into another saddle point given by  $A_\mu^{(2)} = -A_\mu^{(1)\dagger}$  with a corresponding connection between the actions of the two configurations:  $S^{(2)} = S^{(1)*}$ . However, some field configurations are themselves  $\mathcal{CK}$ -symmetric in that  $-A_\mu^\dagger$  is equivalent to  $A_\mu$  under a gauge

transformation. If a saddle point is  $\mathcal{CK}$  symmetric, then its action and effective potential are necessarily real. A quick direct proof can be given: For such a field configuration, it is easy to prove that every Wilson loop is real and thus  $\det(\mu, A_\mu)$  is real and positive for a  $\mathcal{CK}$ -symmetric field configuration. If a single  $\mathcal{CK}$ -symmetric saddle point dominates the effective potential, then the sign problem is solved, at least for a particular phenomenological model. Such  $\mathcal{CK}$ -symmetric saddle points have been seen before in finite density calculations [16–19].

Let us consider the Polyakov loop  $P$ , a special kind of Wilson loop, associated with some particular field configuration that is  $\mathcal{CK}$ -symmetric. We can transform to Polyakov gauge where  $A_4$  is diagonal and time-independent, and work with the eigenvalues  $\theta_j$  defined by

$$P(\vec{x}) = \text{diag} [e^{i\theta_1(\vec{x})}, \dots, e^{i\theta_N(\vec{x})}] \quad (11)$$

where the  $\theta_j$ 's are complex but satisfy  $\sum_j \theta_j = 0$ . Because we are primarily interested in constant saddle points, we suppress the spatial dependence hereafter. Invariance under  $\mathcal{CK}$  means that the set  $\{-\theta_j^*\}$  is equivalent to the  $\{\theta_j\}$  although the eigenvalues themselves may permute. In the case of  $SU(3)$ , we may write this set uniquely as

$$\{\theta - i\psi, -\theta - i\psi, 2i\psi\}. \quad (12)$$

This parametrizes the set of  $\mathcal{CK}$ -symmetric  $SU(3)$  Polyakov loops. Notice that both

$$\text{Tr}_F P = e^\psi 2 \cos \theta + e^{-2\psi} \quad (13)$$

and

$$\text{Tr}_F P^\dagger = e^{-\psi} 2 \cos \theta + e^{2\psi} \quad (14)$$

are real, but they are equal only if  $\psi = 0$ . In the usual interpretation of the Polyakov loop expectation value, this implies that the free energy change associated with the insertion of a fermion is different from the free energy change associated with its antiparticle. It is easy to check that the trace of all powers of  $P$  or  $P^\dagger$  are all real, and thus all group characters are real as well. This parametrization represents a generalization of the Polyakov loop parametrization used in the application of mean-field methods to confinement, *e.g.*, in PNJL models [20] or in gauge theories with double-trace deformations [21, 22]. This parametrization can be generalized to include finite density models for arbitrary  $N$ .

The existence of complex  $\mathcal{CK}$ -symmetric saddle points provides a fundamental approach to non-Abelian gauge theories that is similar to the heuristic introduction of color chemical potentials, and naturally ensures the system has zero color charge, *i.e.*, all three charges contribute equally [23]. In the case of  $SU(3)$ , extremization of the thermodynamic potential with respect to  $\theta$  leads to the requirement  $\langle n_r \rangle - \langle n_g \rangle = 0$  where  $\langle n_r \rangle$  is red color density, including the contribution of gluons. Similarly, extremization of the thermodynamic potential with respect to  $\psi$  leads  $\langle n_r \rangle + \langle n_g \rangle - 2\langle n_b \rangle = 0$ . Taken together, these two relations imply that  $\langle n_r \rangle = \langle n_g \rangle = \langle n_b \rangle$ .

We demand that any saddle point solution be stable to constant, real changes in the Polyakov loop eigenvalues, corresponding for  $SU(3)$  to constant real changes in  $A_4^3$  and  $A_4^8$ . Consider the  $(N-1) \times (N-1)$  matrix  $M_{ab}$ , defined in Polyakov gauge as

$$M_{ab} \equiv g^2 \frac{\partial^2 V_{eff}}{\partial A_4^a \partial A_4^b}. \quad (15)$$

At very high temperatures and densities, the eigenvalues of this mass matrix give the usual Debye screening masses. The stability criterion is that the eigenvalues of  $M$  must have positive real parts. At  $\mathcal{CK}$ -symmetric saddle points, the eigenvalues will be either real or part of a complex conjugate pair. In the case of  $SU(3)$ , the matrix  $M$  may also be written in terms of derivatives with respect to  $\theta$  and  $\psi$  as

$$M = \frac{g^2}{T^2} \begin{pmatrix} \frac{1}{4} \frac{\partial^2 V_{eff}}{\partial \theta^2} & \frac{i}{4\sqrt{3}} \frac{\partial^2 V_{eff}}{\partial \theta \partial \psi} \\ \frac{i}{4\sqrt{3}} \frac{\partial^2 V_{eff}}{\partial \theta \partial \psi} & \frac{-1}{12} \frac{\partial^2 V_{eff}}{\partial \psi^2} \end{pmatrix}. \quad (16)$$

This stability criterion generalizes the stability criterion used previously for color chemical potentials, which was  $\partial^2 V_{eff} / \partial \psi^2 < 0$ . Crucially, the mass matrix  $M_{ab}$  is invariant under  $M^* = \sigma_3 M \sigma_3$ , which is itself a generalized  $\mathcal{PT}$  (parity-time) symmetry transformation [14, 15]. It is easy to see that this relation implies that  $M_{ab}$  has either two real eigenvalues or a complex eigenvalue pair. In either case, the real part of the eigenvalues must be positive for stability. In the case where there are two real eigenvalues, we will denote by  $\kappa_1$  and  $\kappa_2$  the two positive numbers such that  $\kappa_1^2$  and  $\kappa_2^2$  are the eigenvalues of the mass matrix  $M_{ab}$ . If  $M_{ab}$  has two complex eigenvalues, we define two positive real numbers  $\kappa_R$  and  $\kappa_I$  such that  $(\kappa_R \pm i\kappa_I)^2$  are the conjugate eigenvalues of  $M_{ab}$ . The border separating the region  $\kappa_I \neq 0$  from the region  $\kappa_I = 0$  is known as the disorder line [24–26]. In this case, it separates the region where the color density correlation function decays exponentially in the usual way from the region where a sinusoidal modulation is imposed on that decay.

We illustrate the working of  $\mathcal{CK}$  symmetry using the well-known one-loop expressions for the effective potential of particles moving in a constant background Polyakov loop. The one-loop contribution to the effective potential of  $N_f$  flavors of fundamental fermions moving in a background gauge field  $A$  is given by

$$\beta\mathcal{V}V_{eff}^f = -N_f \log [\det (\mu, A)] \quad (17)$$

where  $\det$  again represents the functional determinant of the Dirac operator and  $\beta\mathcal{V}$  is the volume of spacetime. A compact expression for the effective potential of massless fermions when the eigenvalues of  $P$  are complex was derived using zeta function methods in [27]. The finite temperature contribution to the effective potential from quarks is given by

$$V_f^T(P) = -2TN_f \int \frac{d^3k}{(2\pi)^3} \text{Tr}_F [\log (1 + e^{\beta\mu - \beta\omega_k} P) + \log (1 + e^{-\beta\mu - \beta\omega_k} P^\dagger)] \quad (18)$$

where  $\omega_k = +\sqrt{k^2 + m^2}$  with  $m$  the fermion mass. We have evaluated  $V_f(P)$  analytically for the case of massless quarks [11]. The result for quarks in a  $\mathcal{CK}$ -symmetric  $SU(3)$  background Polyakov loop is

$$V_f^T(\theta, \psi, T, \mu) = N_f \left( v_f \left( \theta - i\psi - \frac{i\mu}{T} \right) + v_f \left( -\theta - i\psi - \frac{i\mu}{T} \right) + v_f \left( 2i\psi - \frac{i\mu}{T} \right) \right) \quad (19)$$

where

$$v_f(\theta) = -\frac{4T^4}{\pi^2} \left( \frac{\theta^4}{48} - \frac{\pi^2\theta^2}{24} + \frac{7\pi^4}{720} \right). \quad (20)$$

Explicitly, this is

$$\begin{aligned} V_f^T(\theta, \psi, T, \mu) = & -\frac{\mu^4}{2\pi^2} + T^2 \left( -\mu^2 + \frac{2\theta^2\mu^2}{\pi^2} - \frac{6\mu^2\psi^2}{\pi^2} \right) + \frac{4T^3(\theta^2\mu\psi + \mu\psi^3)}{\pi^2} \\ & + \frac{T^4(-7\pi^4 + 20\pi^2\theta^2 - 10\theta^4 - 60\pi^2\psi^2 + 60\theta^2\psi^2 - 90\psi^4)}{30\pi^2}. \end{aligned} \quad (21)$$

for two flavors of massless quarks. This is manifestly real. Because we are interested in the analytic continuation of Polyakov loop eigenvalues into the complex plane, we need expressions for the gauge bosons as well as for fermions. In our previous work, we have shown that for  $SU(3)$

$$V_g(P) = \frac{T^4 \left( 135(\theta^2 - 3\psi^2)^2 + 180\pi^2(\theta^2 - 3\psi^2) + 60\pi\theta(27\psi^2 - 5\theta^2) - 16\pi^4 \right)}{90\pi^2} \quad (22)$$



which is also manifestly real. Note that the valid range of  $\theta$  is  $(0, \pi)$  due to the appearance of  $2\theta$  as an eigenvalue in the adjoint representation. The one-loop effective potential is simply the sum of  $V_g(\theta)$  and  $V_f(\theta)$ . As is the case when  $\mu = 0$ , the dominant saddle point remains at  $\theta = 0$  when  $\mu \neq 0$ : the one-loop effective potential incorrectly predicts that QCD is always in the extreme deconfined phase with  $\text{Tr}_F P = \text{Tr}_F P^\dagger = 3$  because there is no confinement mechanism included.

#### IV. MODELS

We now consider a class of phenomenological models that combines the one-loop result with the effects of confinement for the case of  $SU(3)$  gauge bosons and two flavors of quarks at finite temperature and density. The model is described by an effective potential which is the sum of three terms:

$$V_{eff}(P) = V_g(P) + V_f(P) + V_d(P). \quad (23)$$

The potential term  $V_g(P)$  is the one-loop effective potential for gluons given by eqn. (22). The potential term  $V_f(P)$  contains all quark effects, including the one-loop expression defined above in eqn. (18). The potential term  $V_d(P)$  represents confinement effects. We will consider three different forms for  $V_f(P)$  and two different forms for  $V_d(P)$  for a total of six different models. The formulas and parameters we use for these models are summarized in Tables I and II.

The potential term  $V_d(P)$  acts to favor the confined phase at low temperature and density [12, 21, 28, 29]. There are two different points of view that can be taken on this potential. In one view,  $V_d(P)$  represents a deformation added to the original model, and hence the subscript  $d$ . In typical applications, the temperature  $T$  is taken to be large such that perturbation theory is reliable in the chromoelectric sector because the running coupling  $g^2(T)$  is small. The deformation term is taken to respect center symmetry and is used to move between the confined and deconfined phases in a controlled way. The gauge contribution  $V_g(P)$  favors the deconfined phase, and in the pure gauge theory ( $N_f = 0$ ) the deconfinement transition arises out of the competition between  $V_g(P)$  and  $V_d(P)$ . The confined phase arising in models of this type is known to be analytically connected to the usual low-temperature confined phase of  $SU(3)$  gauge theory [21]. This point of view emphasizes analytic control at the price of deforming the original gauge theory by the addition of  $V_d(P)$ . In the

second point of view,  $V_d$  is phenomenological in nature and models the unknown confining dynamics of the pure gauge theory. The parameters of  $V_d(P)$  are set to reproduce the deconfinement temperature of the pure gauge theory, known from lattice simulations to occur at  $T_d \approx 270$  MeV.

We will take the second point of view, using simple expressions for  $V_d(P)$  that reproduces much of the thermodynamic behavior seen in lattice simulations of the pure gauge theory. The specific form used are Model A and Model B of [12]. In Model A,  $V_d(P)$  can be written as

$$V_d^A(P) = \sum_{j,k=1}^N \left(1 - \frac{1}{N} \delta_{jk}\right) \frac{M_A^2}{2\beta^2} B_2 \left( \frac{\Delta\theta_{jk}}{2\pi} \right) \quad (24)$$

where  $\Delta\theta_{jk} = |\theta_j - \theta_k|$  are the adjoint Polyakov loop eigenvalues and  $B_2$  is the second Bernoulli polynomial. This expression gives a simple quartic polynomial in the Polyakov loop eigenvalues for  $V_g(P) + V_d^A(P)$  and thus can be thought of as a form of Landau-Ginsburg potential for the Polyakov loop eigenvalues. For the  $SU(3)$  parametrization used here,  $V_d^A(P)$  takes the simple form

$$V_d^A(P) = \frac{M_A^2 T^2 ((2\pi - 3\theta)^2 - 27\psi^2)}{6\pi^2}. \quad (25)$$

The parameter  $M_A$  controls the location of the deconfinement transition in the pure gauge theory, and is set to 596 MeV. At low temperatures, this term dominates the pure gauge theory effective potential. The variable  $\psi$  is zero, and  $V_d(P)$  is minimized when  $\theta = 2\pi/3$ . For this value of  $\theta$ , the eigenvalues of  $P$  are uniformly spaced around the unit circle, respecting center symmetry, and  $\text{Tr}_F P = \text{Tr}_F P^\dagger = 0$ . As the temperature increases,  $V_g(P)$  becomes relevant, and gives rise to the deconfined phase where center symmetry is spontaneously broken. The addition of light fundamental quarks via  $V_f(P)$  explicitly breaks center symmetry. For all nonzero temperatures, center symmetry is broken and  $\langle \text{Tr}_F P \rangle \neq 0$ . However, a remnant of the deconfinement transition remains in the form of a rapid crossover from smaller value of  $\text{Tr}_F P$  to larger ones as  $T$  and  $\mu$  are varied. We also use Model B, defined as

$$V_d^B(P) = -\frac{T}{R^3} \log \left[ \prod_{j < k} \sin^2 \left( \frac{\theta_j - \theta_k}{2} \right) \right]. \quad (26)$$

This form for  $V_d$  is motivated by Haar measure, representing a determinantal term that tries to keep a space-time volume of order  $\beta R^3$  confined. For the  $SU(3)$  parametrization,  $V_d^B(P)$

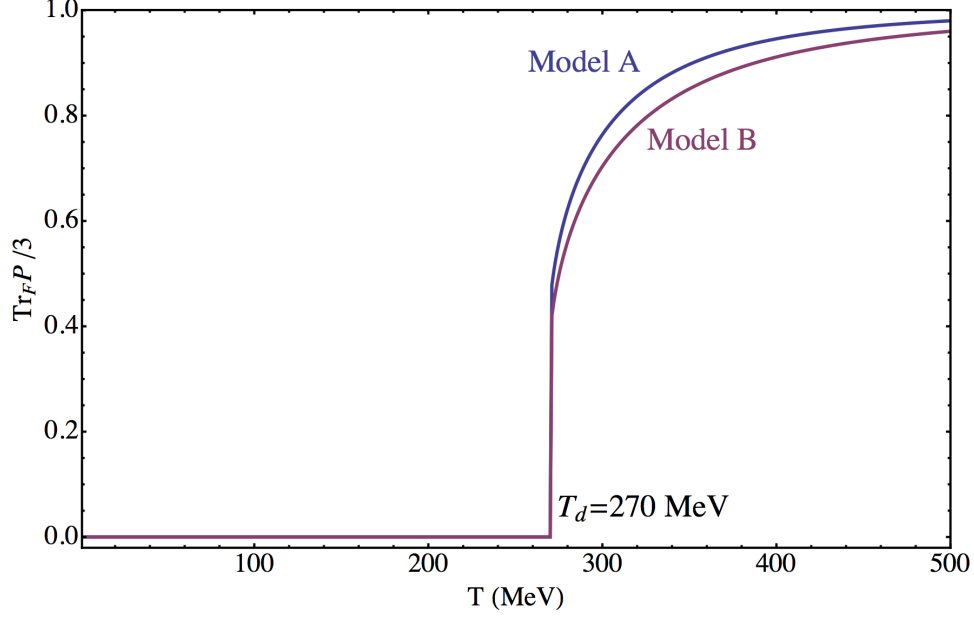


Figure 1:  $\langle \text{Tr}_F P \rangle$  as a function of  $T$  for pure  $SU(3)$  with Model A and Model B for confinement effects.

takes the form

$$V_d^B(P) = -\frac{T}{R^3} \log \left[ \frac{1}{4} \{ \cos \theta - \cosh(3\psi) \}^2 \sin^2 \theta \right]. \quad (27)$$

In order to reproduce the correct deconfinement temperature for the pure gauge theory,  $R$  must be set to  $R = 1.0028$  fm. We plot the Polyakov loop for both Model A and Model B in Fig. 1.

Although  $V_d^A$  and  $V_d^B$  appear to be very different, and are motivated in different ways, they are actually closely related. The deformation potential  $V_d^A$  can also be written as

$$V_d^A = \frac{M_A^2 T^2}{2\pi^2} \sum_{n=1}^{\infty} \frac{1}{n^2} \text{Tr}_A P^n \quad (28)$$

while  $V_d^B$  can be written as

$$V_d^B = \frac{T}{R^3} \sum_{n=1}^{\infty} \frac{1}{n} \text{Tr}_A P^n. \quad (29)$$

Using  $\text{Tr}_A P = \text{Tr}_F P^n \text{Tr}_F P^{\dagger n} - 1$ , it is easy to prove that minimizing either  $V_d^A$  or  $V_d^B$  yields a confining phase where  $\text{Tr}_F P^n = 0$  for all  $n \neq 0 \text{ mod}(N)$ .

We consider three different cases of quarks. The first is heavy quarks, with a fixed mass of 2 GeV. The form of  $V_f(P)$  is precisely that of Eq. (18) with the fermion mass set to a large value. In this model, the quarks are essentially irrelevant for the deconfinement

Model of confinement	Confining potential $V_d$	Parameter
A	Eq. (25)	$M_A = 596 \text{ MeV}$
B	Eq. (27)	$R = 1.0028\text{fm}$

Table I: Potential term and parameters for modeling confinement effects. Parameters are determined from the deconfinement temperature for pure  $SU(3)$  gauge theory.

Model of $N_f = 2$ fermions	Quark potential $V_f$	$m_0$	$g_S$	$\Lambda$
Heavy Quarks	Eq. (40)	2000 MeV	0	-
Massless Quarks	Eq. (21)	0	0	-
PNJL	Eq. (38) + Eq. (40)	5.5 MeV	5.496 $\text{GeV}^{-2}$	631.4 MeV

Table II: Potential term and parameters for quark sector. All numerical values are for two-flavor QCD.

transition, which occurs at essentially the same temperature as if no quarks were present at all. The effect of spontaneous chiral symmetry breaking is not included, as it would only contribute a small amount to the quark mass. This case is in some sense the simplest, and perhaps would be the easiest for which to obtain reliable simulation results. The second case considered is massless quarks, where the fermion mass in Eq. (18) is set equal to zero. This case cannot be easily simulated using lattice methods, because it ignores chiral symmetry breaking effects which do occur in lattice simulations. It is thus useful only for sufficiently large values of  $T$  and  $\mu$  such that chiral symmetry is essentially restored. Our most realistic treatment of quarks uses a Nambu-Jona Lasinio four-fermion interaction to model chiral symmetry breaking effects, so these models are of Polyakov-Nambu-Jona Lasinio (PNJL) type [20].

In our PNJL models, we write the fermionic part of the partition function as

$$Z_f = \int \mathcal{D}\bar{\psi} \mathcal{D}\psi e^{i \int d^4x \mathcal{L}_f} \quad (30)$$

using  $N_f = 2$  Nambu-Jona-Lasinio-type Lagrangian with the constant Polyakov loop [20]

$$\mathcal{L}_f = \bar{\psi}(i\gamma \cdot D - m_0)\psi + g_S \left\{ (\bar{\psi}\psi)^2 + (\bar{\psi}i\gamma_5 \lambda^a \psi)^2 \right\} \quad (31)$$

where  $m_0$  is the current mass of the quarks,  $g_S$  is the four-fermion coupling, and  $\lambda^a$ 's are the generators of the flavor symmetry group  $SU(2)$ . The covariant derivative  $D_\mu$  couples

the fermions to a background Polyakov loop via the component of the gauge field in the temporal direction. Introducing auxiliary fields, a scalar field  $\sigma$  and triplet of pseudoscalar fields  $\pi^a$ ,

$$\mathcal{L}_{aux} = -g_S \{ \sigma^2 + (\pi^a)^2 \} + 2g_S \bar{\psi} \{ \sigma + i\gamma_5 \lambda^a \pi^a \} \psi, \quad (32)$$

and integrating over the fermion fields, we can write the partition function in terms of the boson fields (i.e. bosonization)

$$Z_f = \int \mathcal{D}\sigma \mathcal{D}\pi^a \exp \left[ i \int d^4x \{ \text{tr} \log [i\gamma \cdot D - m_0 + 2g_S(\sigma + i\pi^a \lambda^a)] - g_S (\sigma^2 + (\pi^a)^2) \} \right]. \quad (33)$$

We use the background field method for the scalar field,  $\sigma(x) = \sigma_0 + s(x)$  and write the partition function as

$$Z_f = \exp \left[ i \int d^4x \{ \text{tr} \log [i\gamma \cdot D - m] - g_S \sigma_0^2 \} \right] \int \mathcal{D}s \mathcal{D}\pi^a \exp \left[ i \int d^4x \mathcal{L}_b \right] \quad (34)$$

where  $m = m_0 - 2g_S \sigma_0$  is the constituent quark mass  $m$ ,  $\text{tr}$  denotes the trace over the color, flavor, and Dirac space, and the bosonized Lagrangian is

$$\mathcal{L}_b = \text{tr} \log \left[ 1 + \frac{1}{i\gamma \cdot D - m} 2g_S (s + i\pi^a \lambda^a) \right] - g_S (s^2 + (\pi^a)^2). \quad (35)$$

We perform a Wick rotation and consider the theory in Euclidean space from now on. The first term in the partition function (34) gives the effective potential,

$$V_f = V_f^T(P, m) + V_f^0(m, m_0), \quad (36)$$

which consists of the finite-temperature part  $V_f^T$ , which is given by Eq. (18) and the vacuum part  $V_f^0$ ,

$$V_f^0(m, m_0) = \frac{(m - m_0)^2}{4g_S} - 2N_f \text{Tr}_F \int \frac{d^3k}{(2\pi)^3} \omega_k. \quad (37)$$

We note that the finite-temperature contribution  $V_f^T$  is finite for any values of  $P$ ,  $m$ ,  $\mu$ , and  $T$ , while the zero-point energy, the integral in  $V_f^0$ , is divergent and needs a regularization. We use a noncovariant three-dimensional cutoff,  $\Lambda$  [30] and write it as [31]

$$V_f^0(m, m_0) = \frac{(m - m_0)^2}{4g_S} - \frac{N_c N_f \Lambda^4}{8\pi^2} \left\{ \sqrt{1 + (m/\Lambda)^2} [2 + (m/\Lambda)^2] + (m/\Lambda)^4 \log \frac{m/\Lambda}{1 + \sqrt{1 + (m/\Lambda)^2}} \right\}. \quad (38)$$

For  $V_f^T$ , it is often convenient to combine the arguments of the logarithms into a single product that is manifestly real. Using Eq. (18), we can write the finite-temperature effective potential in terms of Polyakov loop eigenvalues as

$$\begin{aligned} V_f^T &= -2TN_f \sum_{j=1}^{N_c} \int \frac{d^3k}{(2\pi)^3} [\log(1 + e^{-(\omega_k - \mu)/T + i\theta_j}) + \log(1 + e^{-(\omega_k + \mu)/T - i\theta_j})] \\ &= -2TN_f \int \frac{d^3k}{(2\pi)^3} \{ \log[1 + 2\cos\theta e^{-(\omega_k - \mu)/T + \psi} + e^{-2(\omega_k - \mu)/T + 2\psi}] \end{aligned} \quad (39)$$

$$+ \log[1 + e^{-(\omega_k - \mu)/T - 2\psi}] + (z \rightarrow -z) \} \quad (40)$$

where the last part denotes the antiparticle contribution which has the opposite sign for the chemical potential and the Polyakov loop eigenvalues,  $z = \mu - igA_\mu$ . From this expression, we can see explicitly that the one-loop fermionic effective potential at the complex saddle point is real, independent of any approximation. We use Eqs. (38) and (40) for the effective potential of the fermionic part of PNJL model with the  $T = 0$  parameters taken from [32].

In principle, the coupling of  $P$  and  $\bar{\psi}\psi$  which is a prominent feature of PNJL models can lead to an extended mass matrix that incorporates mixing of  $\bar{\psi}\psi$  with excitations of the Polyakov loop. The kinetic term of the scalar field  $s$  in the bosonized Lagrangian is needed for a full treatment. Using the log expansion and the derivative expansion for Eq. (35) [30, 33], we can obtain the kinetic term for the scalar field in the form

$$\mathcal{L}_b \supset 4N_f g_S^2 \text{Tr}_F I_s^{\mu\nu} \partial_\mu s \partial_\nu s$$

where  $I_s^{\mu\nu}$  is, for example, given as the momentum integral in Eq. (7.54) of [30] but the four-momentum  $k_\mu$  is replaced by  $k_\mu + gA_4\delta_{\mu 4}$  for the PNJL model. Using the identity

$$\int \frac{d^3k}{(2\pi)^3} k_i k_j = \int \frac{d^3k}{(2\pi)^3} \frac{k^2 \delta_{ij}}{3}$$

and rescaling  $s$  for the physical constituent mass, we can write the spatial part of the kinetic term as

$$\mathcal{L}_b \supset \frac{1}{2} I_s [\partial_i (-2g_S s)]^2$$

with

$$\begin{aligned} I_s &= N_f T \sum_{n=-\infty}^{\infty} \int \frac{d^3k}{(2\pi)^3} \text{Tr}_F \left[ \left\{ \frac{2}{[(\omega_n + iz)^2 + \omega_k^2]^2} - \frac{\frac{4}{3}k^2 + 4m^2}{[(\omega_n + iz)^2 + \omega_k^2]^3} \right. \right. \\ &\quad \left. \left. + \frac{\frac{16}{3}k^2 m^2}{[(\omega_n + iz)^2 + \omega_k^2]^4} \right\} + (z \rightarrow -z) \right] \end{aligned} \quad (41)$$

where  $z = \mu - igA_4$  and the summation is over the Matsubara frequencies,  $\omega_n = (2n+1)\pi$ . A similar expression for  $I_s$  is obtained in [34] for the PNJL model. We first use the prescription (12) for the Polyakov loop and sum over the Matsubara frequencies and integrate over the three-momentum in Eq. (41). However, the integral is divergent, and we use the same non-covariant three-dimensional cutoff  $\Lambda$  used for the zero-point energy (38). With the  $s$  kinetic term given in terms of  $I_s$ , we can in principle compute the eigenvalues of an extended mass matrix. It turns out, however, that the off-diagonal coupling of the chiral component of the mass matrix is numerically negligible compared to the Polyakov-loop parts of the mass matrix, and thus we ignore the chiral component in the remainder of this paper.

## V. HEAVY QUARKS

We consider the case of heavy quarks propagating in constant Polyakov loop background. For such quark, the chiral symmetry effects are negligible and a first-order deconfinement transition line is the only true critical behavior found in the phase diagram. Our study of heavy quarks is perhaps most relevant for lattice studies of static quarks at non-zero  $\mu$ ; this approximation is particularly tractable [35].

The center symmetry of pure gauge theory is exact for infinitely heavy quarks. However, quarks with finite mass break the center symmetry explicitly and weaken the first order transition of pure gauge theory. At sufficiently low quark mass the first order transition for deconfinement vanishes at a critical end point. The location of this critical end point is model dependent and has been proposed as a useful way to differentiate between different models of confinement [36]. In both Model A and Model B, the first order deconfinement transition vanishes for quark mass of around 1.5 GeV or less. Therefore we set the quark mass to be 2 GeV so that the deconfinement transition still persists. The end point of the deconfinement transition line lies at smaller values of  $\mu$ , and appears to play no direct role in the behavior of  $\psi$  and  $\kappa_I$ . The quark mass is large compared to the confinement scale, so asymptotic freedom applies in the region  $\mu \simeq m$ . In this region, perturbation theory is a reliable guide when  $T \gg T_d$ , the pure gauge deconfinement temperature. However, below  $T_d$ , non-perturbative confinement effects cannot be neglected, hence the importance of the potential term  $V_d$  beyond what is usually considered the confining region at low  $T$  and  $\mu$ . A useful expansion for  $\beta(m - \mu) \gg 1$  can be generated by expanding the logarithm in

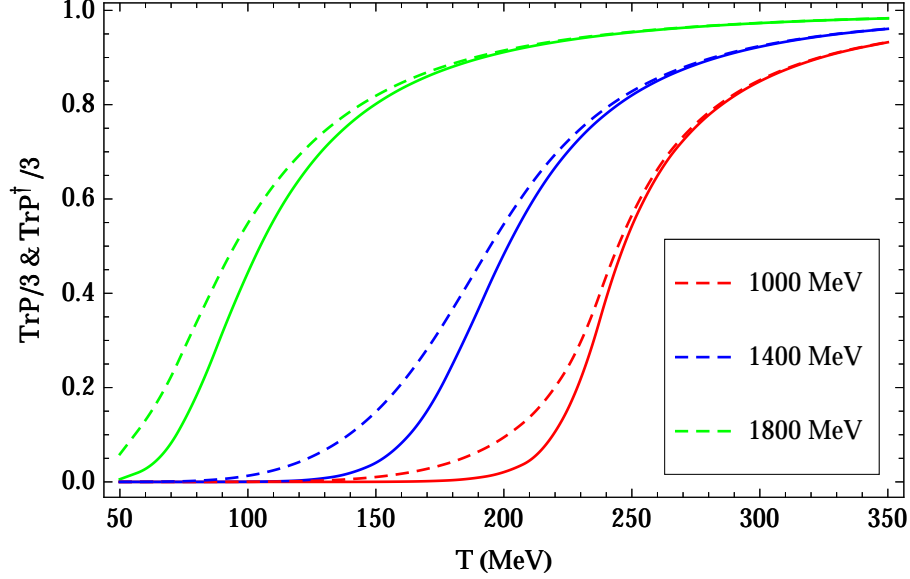


Figure 2:  $\langle \text{Tr}_F P \rangle$  and  $\langle \text{Tr}_F P^\dagger \rangle$  as a function of  $T$  for  $\mu = 1000, 1400$  and  $1800$  MeV for heavy quarks using Model A for confinement effects. The Polyakov loops are normalized to one as the temperature becomes large.

Eq. (18) and integrating term by term [37]. Such an expansion gives

$$V_f(P) = \sum_{n=1}^{\infty} \frac{(-1)^n m^2 T^2}{n^2 \pi^2} K_2(n\beta m) (e^{\frac{n\mu}{T}} \text{Tr}_F P^n + e^{-\frac{n\mu}{T}} \text{Tr}_F P^{\dagger n}). \quad (42)$$

At low temperature and density the effects of heavy quarks can be obtained approximately from the  $n = 1$  term of Eq. (42). However, this expansion fails in the high density region ( $\mu > 1.5$  GeV) in case of Model A as can be seen in Fig. 6. In our analysis we have therefore numerically integrated the full one loop expression for heavy quark potential.

In Fig. 2 we show  $\text{Tr}_F P$  and  $\text{Tr}_F P^\dagger$  as a function of  $T$  for various values of  $\mu$  when the heavy quark has a mass of  $2$  GeV. In agreement with our general argument above, the crossover moves toward lower values of  $T$  as  $\mu$  increases. The separation between  $\text{Tr}_F P$  and  $\text{Tr}_F P^\dagger$  is largest in the crossover region, and is negligible at higher temperatures. As shown in the figure, the separation is largest for some intermediate value of  $\mu$  less than the heavy quark mass. The behavior of  $\text{Tr}_F P$  and  $\text{Tr}_F P^\dagger$  for Model B is similar to Model A, as may be seen from Fig. 3. The crossover happens at higher temperature for Model B, showing that the confining effect for Model B is smaller than Model A. Because  $\psi$  is non-zero in both models, there is a difference between  $\text{Tr}_F P$  and  $\text{Tr}_F P^\dagger$ .



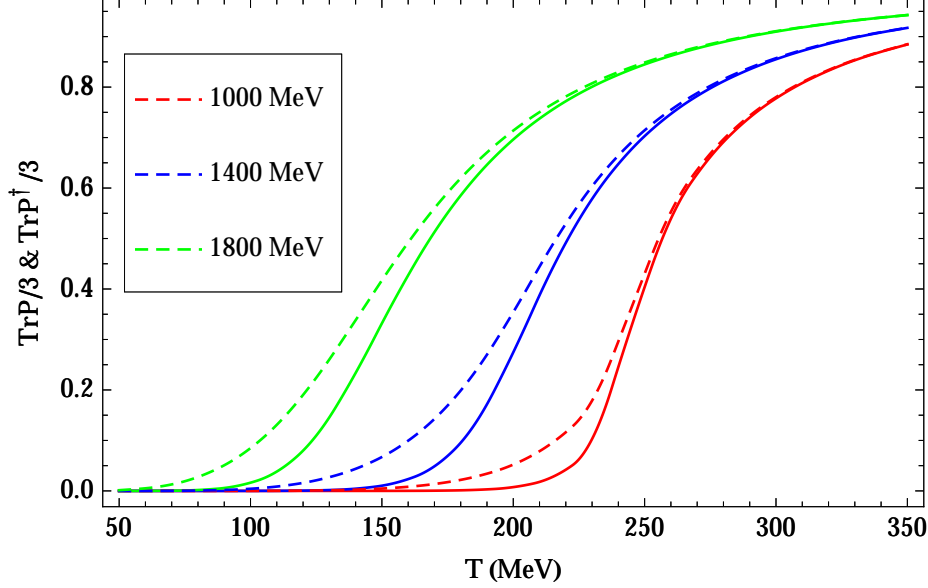


Figure 3:  $\langle \text{Tr}_F P \rangle$  and  $\langle \text{Tr}_F P^\dagger \rangle$  as a function of  $T$  for  $\mu = 1000, 1400$  and  $1800$  MeV for heavy quarks using Model B for confinement effects. The Polyakov loops are normalized to one as the temperature becomes large.

In Fig. 4, we show for Model A a contour plot for  $\psi$  along with a shaded region showing where  $\kappa_I \neq 0$ . The boundary of the shaded region is thus the disorder line. From this graph, we see that values of  $\psi$  are very small, but peak in a region centered roughly around  $\mu = 1500$  MeV and  $T = 150$  MeV. There is no obvious relation between the region where  $\psi$  is largest and the region where  $\kappa_I \neq 0$ . However, the peak in  $\psi$  is located near the point where the disorder line abruptly changes.

Figure 5 again shows the region where  $\kappa_I \neq 0$  and the associated disorder line, but now with contour lines for  $\kappa_I$  added. As with all the contour plots of this type, we have set the running coupling  $\alpha_s(T, \mu) = 1$ . In other words, conversion to the actual one-loop values requires multiplying these values by appropriate values for  $\sqrt{\alpha_s(T, \mu)}$ . The region where the mass eigenvalues  $\kappa_1$  and  $\kappa_2$  form a complex conjugate pair has a complicated shape. The mass matrix eigenvalues are real for  $\mu$  below about 600 MeV. There is a roughly rectangular region for  $600 \text{ MeV} \lesssim \mu \lesssim 1450 \text{ MeV}$ . This is followed by a region where the boundary rises roughly linearly with  $\mu$ , similar to the behavior of Model A with massless quarks.

Figure 6 shows the physics associated with this behavior. The boundary using the complete one-loop expression is compared with both the massless boundary and the boundary

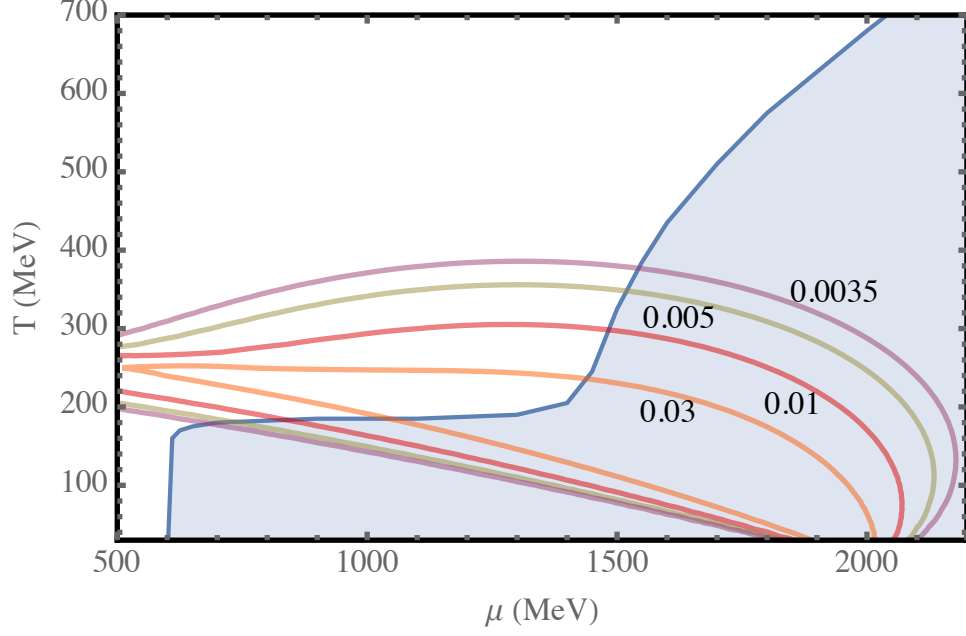


Figure 4: Contour plot of  $\psi$  in the  $\mu - T$  plane for heavy quarks ( $m = 2000$  MeV) using Model A for confinement effects. The region where  $\kappa_I \neq 0$  is shaded.

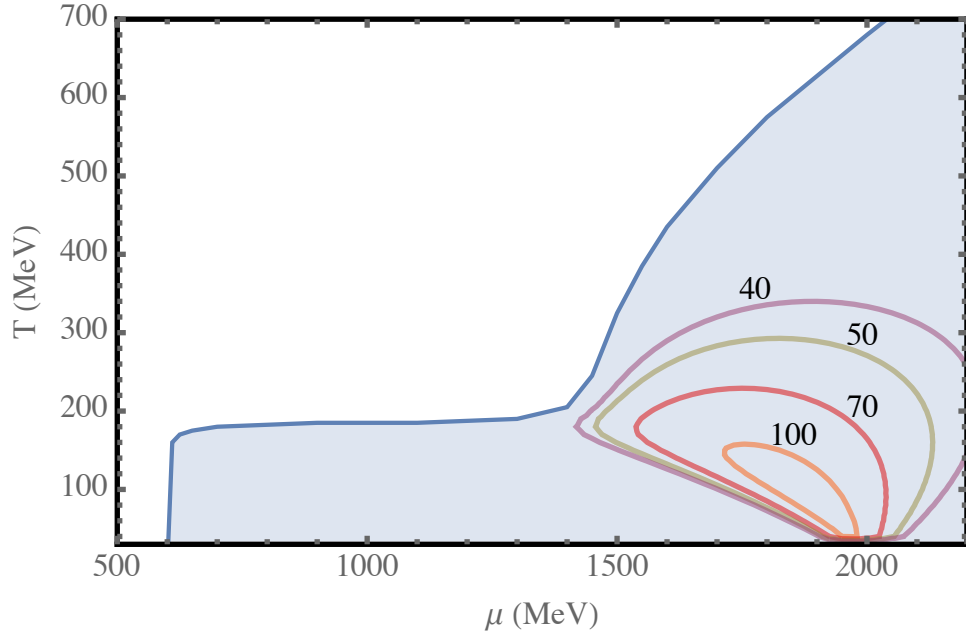


Figure 5: Contour plot of  $\kappa_I$  in the  $\mu - T$  plane for heavy quarks ( $m = 2000$  MeV) using Model A for confinement effects. Contours are given in MeV with  $\alpha_S$  set to one. The region where  $\kappa_I \neq 0$  is shaded.

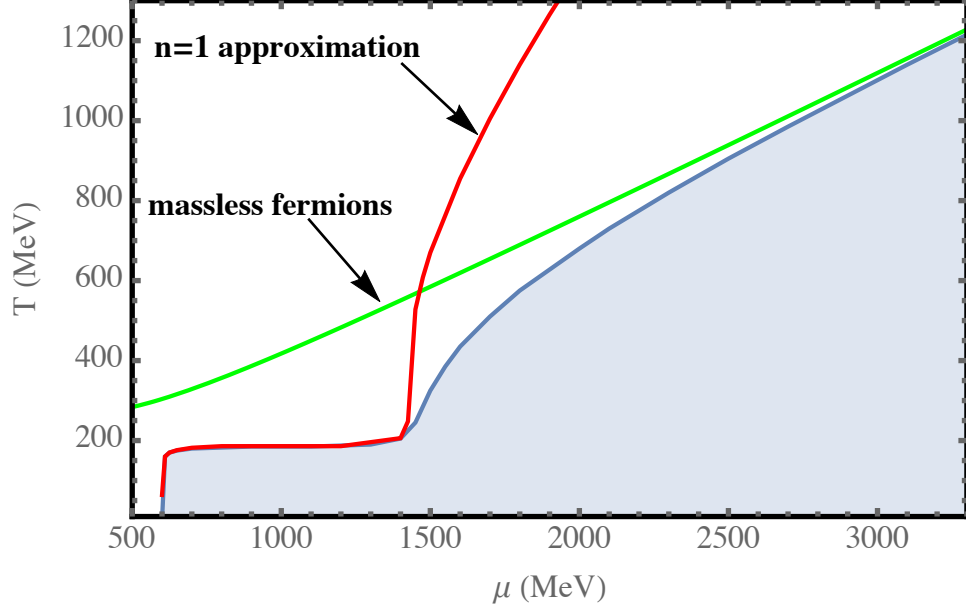


Figure 6: The shaded region indicates where  $\kappa_I \neq 0$  for heavy quarks ( $m = 2000$  MeV) using Model A for confinement effects. The boundary of this region is also shown using an approximation appropriate for very heavy quarks ( $\beta m \gg 1$ ) as well as for massless quarks, appropriate when  $\beta m \ll 1$ .

obtained using the  $n = 1$  approximation from Eqn. 42 to the full one-loop expression. As may be seen, the  $n = 1$  term accounts very well for the low-temperature behavior of the boundary, while the massless quark result is accurate for  $\mu$  above the heavy quark mass. It is clear that the abrupt change of the shaded region represents a rapid crossover from the behavior of a heavy quark to the behavior of a massless quark, occurring over a range of roughly  $3M/4 < \mu < 5M/4$ , with most of the change occurring before  $\mu$  reaches  $M$ .

The behavior of  $\psi$  for Model B, as shown in Figure 7, is similar to the behavior of  $\psi$  for Model A, but the values of  $\psi$  are somewhat larger. The region where the eigenvalues of the mass matrix are complex is shown in Fig. 8. The shape and size of the region is very similar to the rectangular region found for Model A in Fig. 5. However, in the high-temperature region, where  $\mu$  is greater than the quark mass, the region of complex mass eigenvalues is completely missing for Model B. This is consistent with the behavior of Model B for massless quarks, where no complex eigenvalues of the mass matrix were found.

Figure 9 shows a comparison of the regions where  $\kappa_I$  is non-zero for both Model A and Model B. Their shape is very similar for smaller values of  $\mu$ , suggesting that some universal

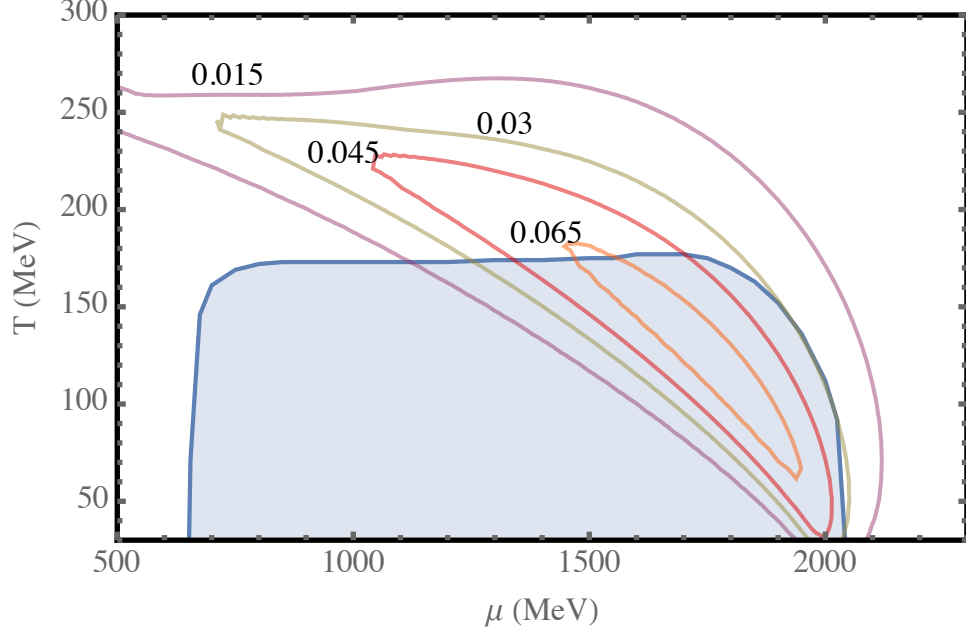


Figure 7: Contour plot of  $\psi$  in the  $\mu - T$  plane for heavy quarks ( $m = 2000$  MeV) using Model B for confinement effects. The region where  $\kappa_I \neq 0$  is shaded.

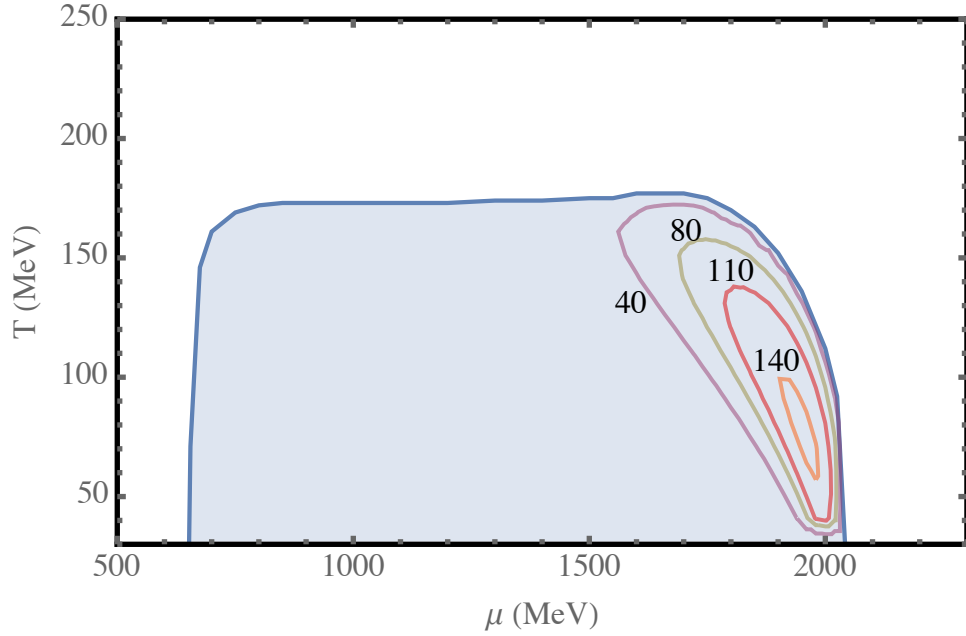


Figure 8: Contour plot of  $\kappa_I$  in the  $\mu - T$  plane for heavy quarks ( $m = 2000$  MeV) using Model B for confinement effects. Contours are given in MeV with  $\alpha_S$  set to one. The region where  $\kappa_I \neq 0$  is shaded.

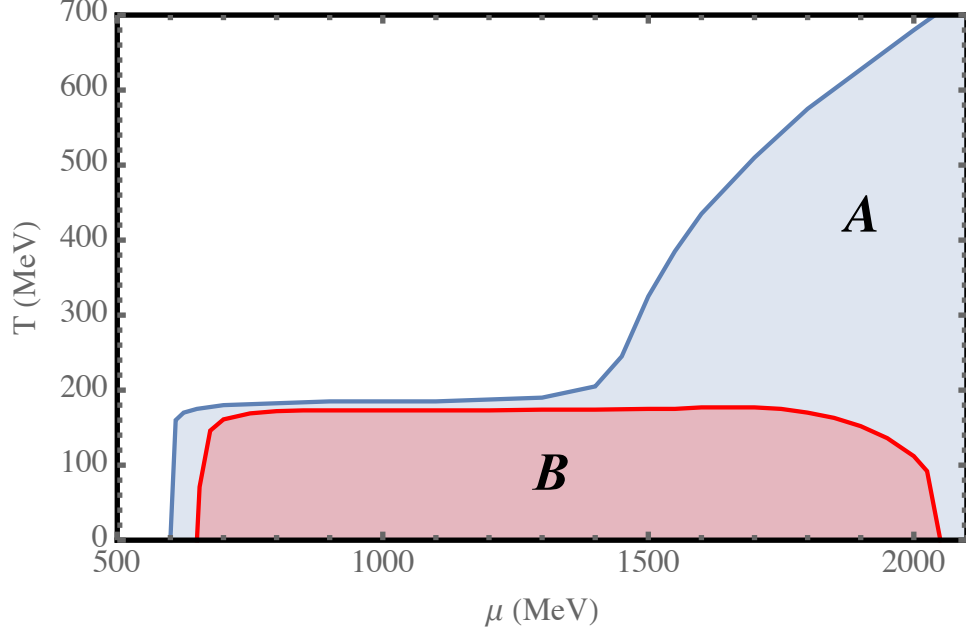


Figure 9: A comparison of the regions where  $\kappa_I \neq 0$  for heavy quarks with Model A and Model B along with the corresponding disorder lines.

behavior occurs in this region. However, the behavior is very different in the region where both  $T$  and  $\mu$  are becoming large. Model A shows a continuation of the disorder line that follows the behavior for massless quarks, while for Model B the disorder line covers a finite region in  $\mu - T$  space.

## VI. MASSLESS QUARKS WITHOUT CHIRAL EFFECTS

In this section we extend the results of our previous work on massless quarks using Model A [11], including more detail and providing a comparison with Model B. This simple model where the quark mass  $m$  is set to zero neglects chiral symmetry breaking, relevant at low  $T$  and low  $\mu$ . It should not be expected to reproduce exactly the features seen in lattice simulations. Nevertheless, comparison with PNJL model results, *e.g.*, [38], show that the model is quantitatively similar to the behavior of models with many more free parameters that include chiral symmetry effects. For Model A,  $\text{Tr}_F P$  shows a slightly larger initial rise in  $\text{Tr}_F P$  with temperature than does the model studied in [38]. This is consistent with the role that chiral symmetry breaking plays in diminishing the explicit breaking of  $Z(3)$  symmetry by quarks.

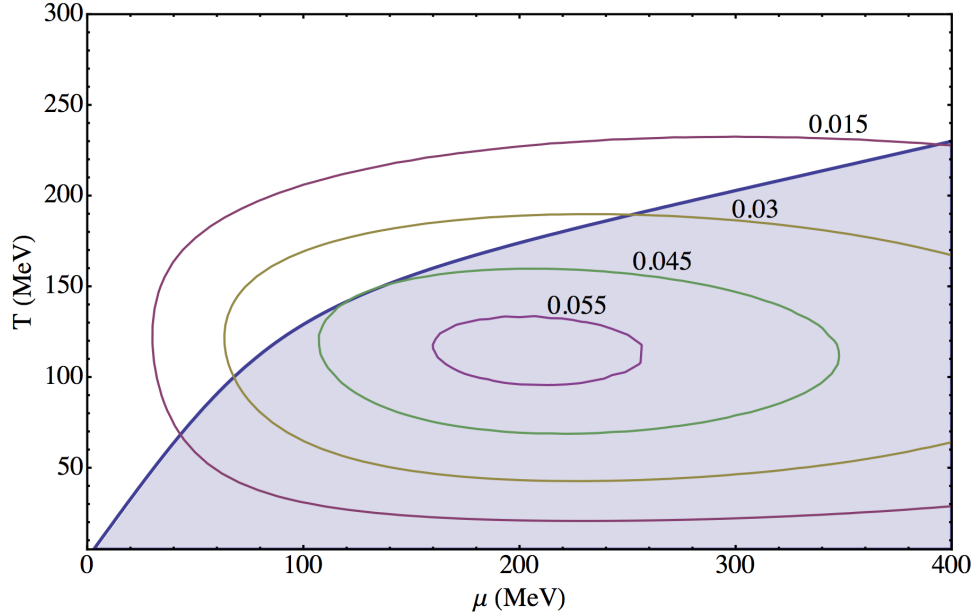


Figure 10: Contour plot of  $\psi$  in the  $\mu - T$  plane for Model A with massless quarks, showing where  $\text{Tr}_F P$  is most different from  $\text{Tr}_F P^\dagger$ . The region where  $\kappa_I \neq 0$  is shaded.

Figure 10 shows the region for Model A where  $\kappa_I$  is non-zero superimposed on a contour plot of  $\psi$ , while 11 shows contour lines for  $\kappa_I$ . Comparison of the two figures shows that the peak in  $\psi$  occurs at a lower value of  $\mu$  than the peak in  $\kappa_I$ , with the peak in  $\psi$  occurring near  $(\mu = 200 \text{ MeV}, T = 110 \text{ MeV})$ . The behavior of the disorder line for large  $T$  and  $\mu$  is known analytically [11]:

$$T = \frac{2\mu}{\sqrt{3}\pi}. \quad (43)$$

This behavior is generic to Model A when  $T, \mu \gg m$ , as we have seen for heavy quarks in the previous section.

The most interesting feature of Model B with massless quarks is that there is no region where  $\kappa_I$  is non-zero. Nevertheless, as shown in Fig. 12,  $\psi$  is non-zero, with a peak value near  $(\mu = 250 \text{ MeV}, T = 140 \text{ MeV})$ . This is the only case we have considered where there is no disorder line.

## VII. PNJL MODELS

In this section we consider our most realistic models of QCD at finite temperature and density, PNJL models evaluated at complex saddle points. These models have a much richer

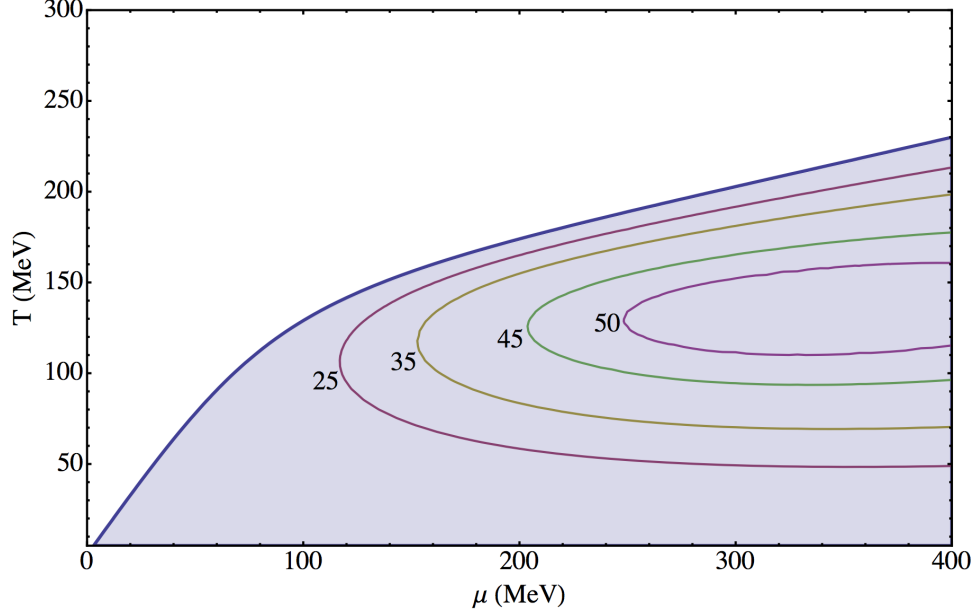


Figure 11: Contour plot of  $\kappa_I$  in the  $\mu - T$  plane for Model A with massless quarks. Contours are given in MeV, with  $\alpha_s$  set to one. The region where  $\kappa_I \neq 0$  is shaded.

structure because the effects of chiral symmetry breaking are included. Because the effective quark mass varies with  $T$  and  $\mu$ , the behavior of the PNJL models in some sense lies between that of the heavy quarks and  $m = 0$  quarks considered in the previous two sections, with a constituent quark mass that varies with  $T$  and  $\mu$ . Figures 13 and 14 show the values of  $\langle \text{Tr}_F P \rangle$ ,  $\langle \text{Tr}_F P^\dagger \rangle$  and  $m$  for a PNJL model using  $V_d^A$  to implement confinement. In all figures of this type, the constituent quark mass  $m$  is normalized to its value at  $(\mu = 0, T = 0)$ , while  $\langle \text{Tr}_F P \rangle$  and  $\langle \text{Tr}_F P^\dagger \rangle$  are normalized so that they go to one as  $T$  goes to infinity. As is typical of PNJL models with appropriately chosen parameters, only crossover behavior is seen at  $\mu = 0$ . There is a critical line starting at  $\mu \approx 350$  MeV when  $T = 0$  and ending at a critical point at approximately  $(\mu \simeq 320$  MeV,  $T \simeq 75$  MeV). This first-order line manifests itself in Fig. 13 in the discontinuous behavior of  $\langle \text{Tr}_F P \rangle$ ,  $\langle \text{Tr}_F P^\dagger \rangle$  and  $m$  at  $T = 50$  MeV.

Figures 15 and 16 show the corresponding behavior of  $\langle \text{Tr}_F P \rangle$ ,  $\langle \text{Tr}_F P^\dagger \rangle$  and  $m$  using  $V_d^B$  to implement confinement. In all figures of this type,  $m$  is normalized to its value at  $(\mu = 0, T = 0)$ , while  $\langle \text{Tr}_F P \rangle$  and  $\langle \text{Tr}_F P^\dagger \rangle$  are normalized so that they go to one as  $T$  goes to infinity. As is Model A, only crossover behavior is seen at  $\mu = 0$ . The critical line starting at  $\mu \approx 350$  MeV when  $T = 0$  ends at a critical point at approximately  $(\mu = 320$  MeV,  $T = 100$  MeV). The first-order line again manifests itself in Fig. 15 in the

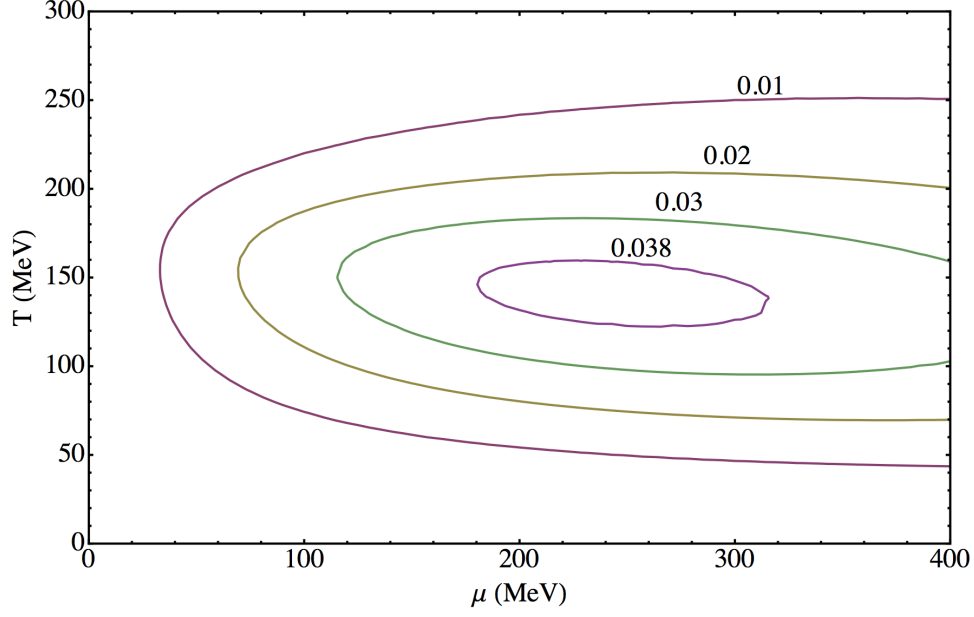


Figure 12: Contour plot of  $\psi$  in the  $\mu - T$  plane for Model B with massless quarks, showing where  $\text{Tr}_F P$  is most different from  $\text{Tr}_F P^\dagger$ .

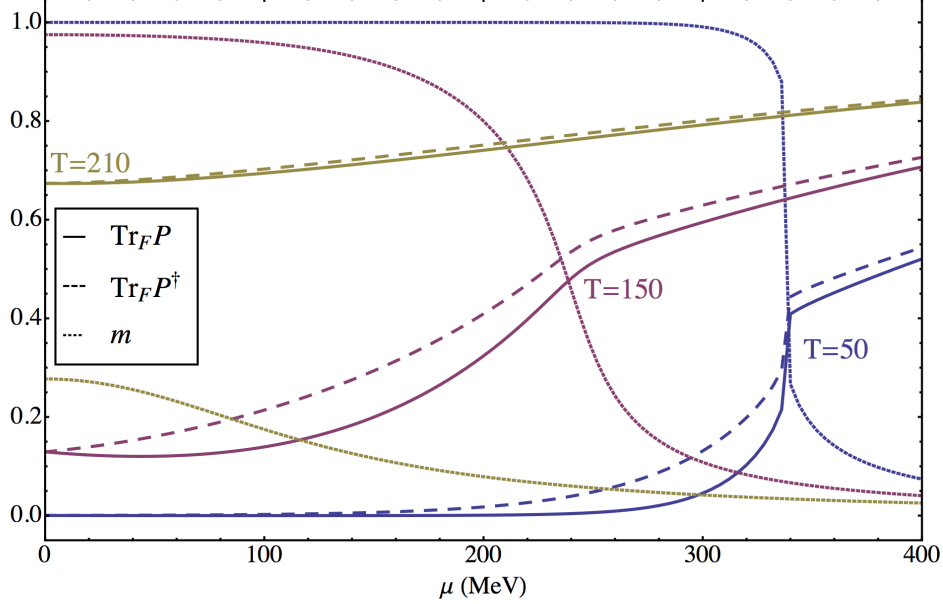


Figure 13: The constituent mass  $m$ ,  $\langle \text{Tr}_F P \rangle$  and  $\langle \text{Tr}_F P^\dagger \rangle$  as a function of  $\mu$  for  $T = 50, 150$ , and  $210$  MeV for a PNJL model using Model A for confinement effects. The constituent mass  $m$  is normalized to one at  $T = 0$ , and the Polyakov loops are normalized to one as the temperature becomes large.



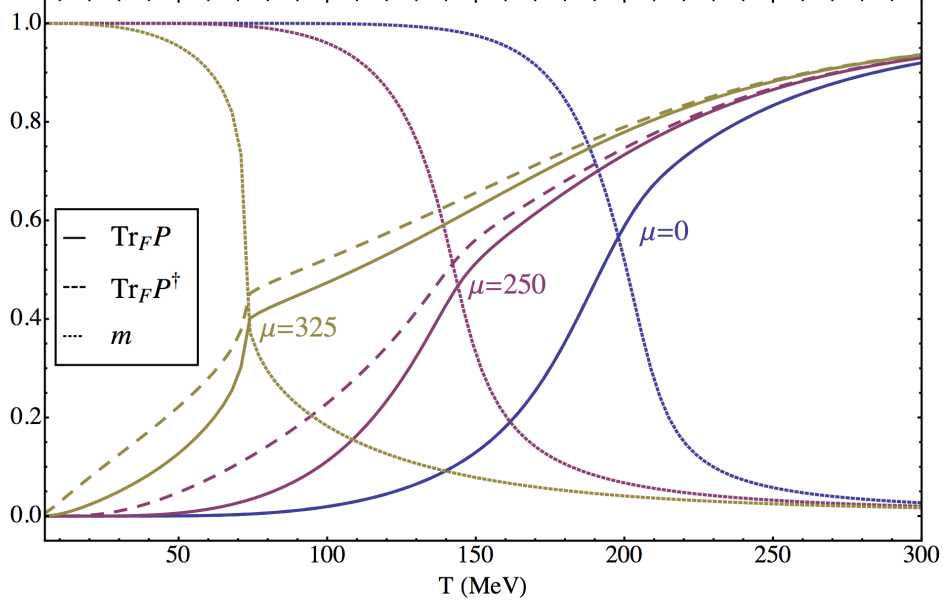


Figure 14: The constituent mass  $m$ ,  $\langle \text{Tr}_F P \rangle$  and  $\langle \text{Tr}_F P^\dagger \rangle$  as a function of  $T$  for  $\mu = 0, 250$  and  $325$  MeV for a PNJL model using Model A for confinement effects. The constituent mass  $m$  is normalized to one at  $T = 0$ , and the Polyakov loops are normalized to one as the temperature becomes large.

discontinuous behavior of  $\langle \text{Tr}_F P \rangle$ ,  $\langle \text{Tr}_F P^\dagger \rangle$  and  $m$  at  $T = 50$  MeV.

Figure 17 shows contour lines for  $\psi$  in the  $\mu - T$  plane along with the region where  $\kappa_I \neq 0$  as well as the critical line. The overall shape of the disorder line is similar to that found in the previous section for heavy quarks, but of course shifted to a much lower value  $\mu$ . The critical line lies completely within the region  $\kappa_I \neq 0$ . Figure 18 shows a contour plot for  $\kappa_I$ . In both figures, a jump in  $\psi$  and  $\kappa_I$  is visible as the critical line is crossed.

As with Model A, the PNJL model using  $V_d^B$  shows many of the same features found for heavy quarks. Figure 19 contour lines for  $\psi$  in the  $\mu - T$  plane along with the region where  $\kappa_I \neq 0$  as well as the critical line, and Figure 20 shows a contour plot for  $\kappa_I$ . A striking difference between Model A and Model B is that the critical line now lies on the boundary of the region  $\kappa_I \neq 0$ , and the disorder line appears to be a smooth continuation of the critical line out of the critical end-point.

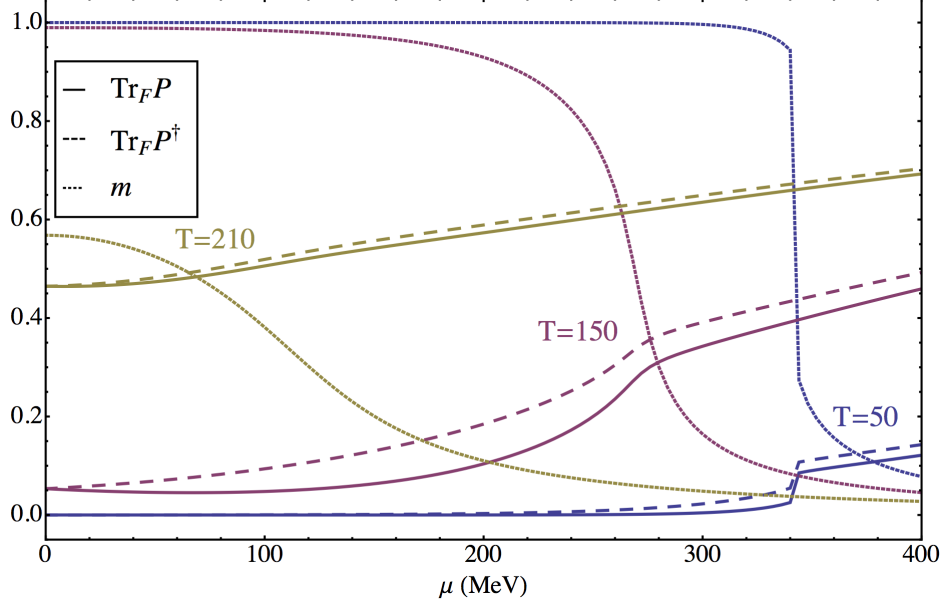


Figure 15: The constituent mass  $m$ ,  $\langle \text{Tr}_F P \rangle$  and  $\langle \text{Tr}_F P^\dagger \rangle$  as a function of  $\mu$  for  $T = 50, 150$ , and  $210$  MeV for a PNJL model using Model B for confinement effects. The constituent mass  $m$  is normalized to one at  $T = 0$ , and the Polyakov loops are normalized to one in the limit as the temperature becomes large.

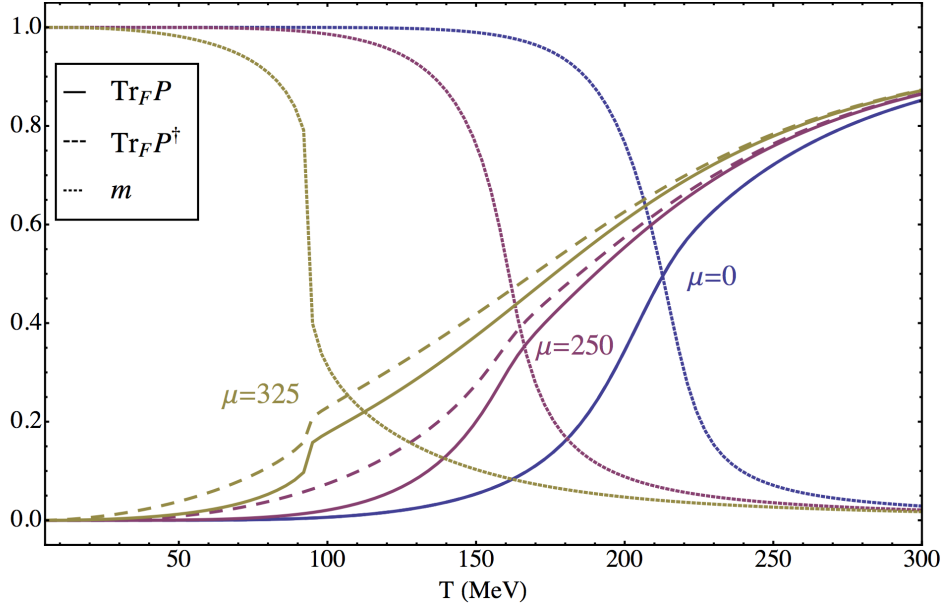


Figure 16: The constituent mass  $m$ ,  $\langle \text{Tr}_F P \rangle$  and  $\langle \text{Tr}_F P^\dagger \rangle$  as a function of  $T$  for  $\mu = 0, 250$  and  $325$  MeV for a PNJL model using Model B for confinement effects. The constituent mass  $m$  is normalized to one at  $T = 0$ , and the Polyakov loops are normalized to one in the limit as the temperature becomes large.

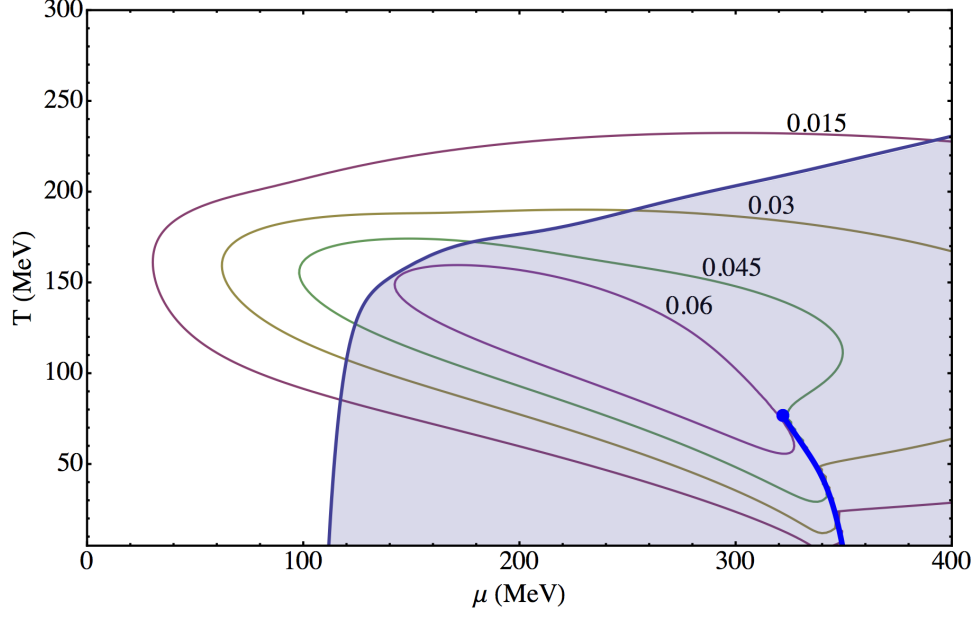


Figure 17: Contour plot of  $\psi$  in the  $\mu - T$  plane for a PNJL model using Model A for confinement effects. The region where  $\kappa_I \neq 0$  is shaded. The critical line and its endpoint are also shown.

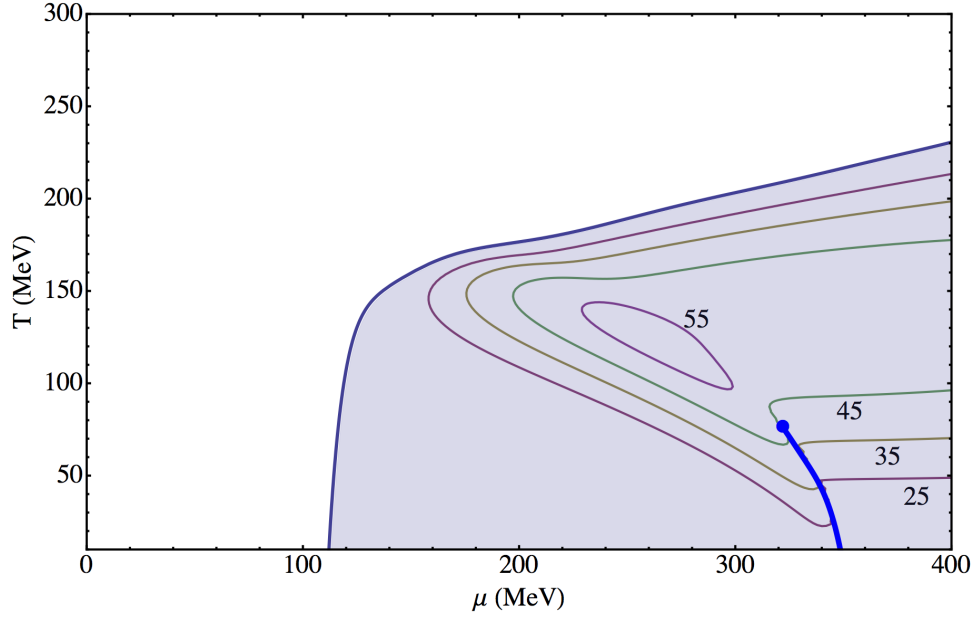


Figure 18: Contour plot of  $\kappa_I$  in the  $\mu - T$  plane for a PNJL model using Model A for confinement effects. Contours are given in MeV, with  $\alpha_s$  set to one. The region where  $\kappa_I \neq 0$  is shaded. The critical line and its endpoint are also shown.

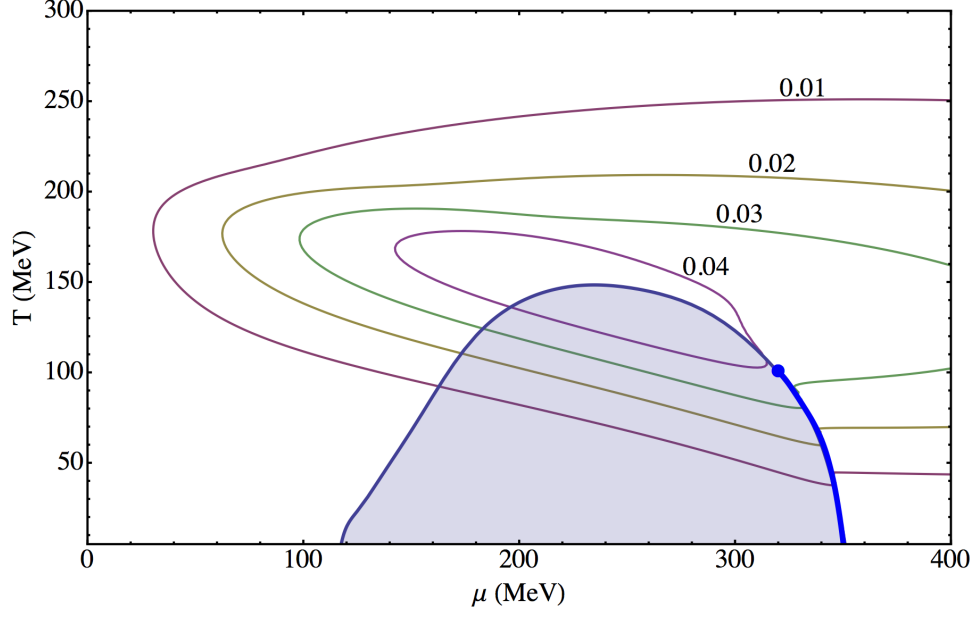


Figure 19: Contour plot of  $\psi$  in the  $\mu - T$  plane for a PNJL model using Model B for confinement effects. The region where  $\kappa_I \neq 0$  is shaded. The critical line and its endpoint are also shown.

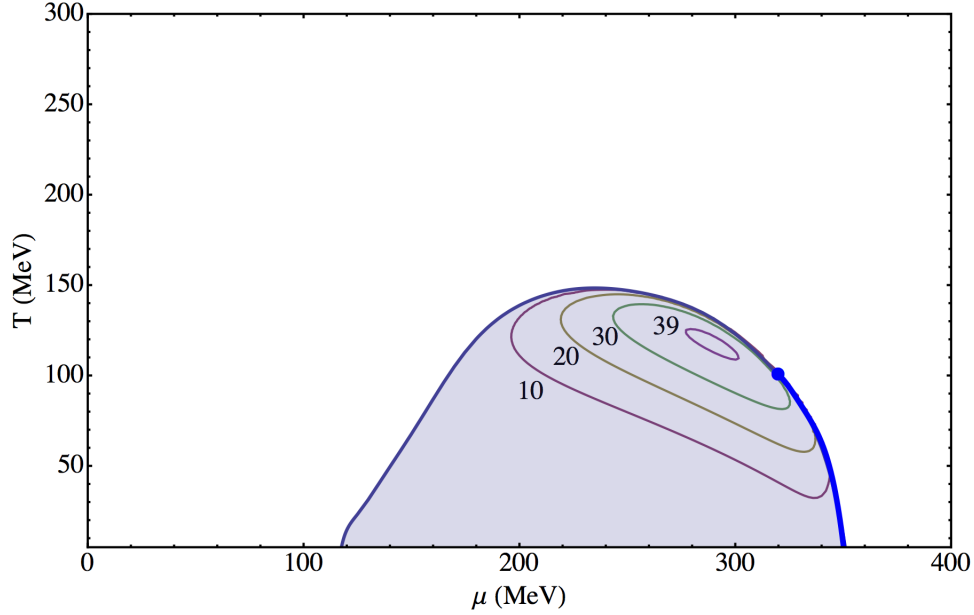


Figure 20: Contour plot of  $\kappa_I$  in the  $\mu - T$  plane for a PNJL model using Model B for confinement effects. Contours are given in MeV, with  $\alpha_s$  set to one. The region where  $\kappa_I \neq 0$  is shaded. The critical line and its endpoint are also shown.

## VIII. CONCLUSIONS

As we have shown, the sign problem in QCD at finite density makes it very desirable to extend real fields into the complex plane. This extension is certainly necessary for steepest descents methods to yield correct results. Complex saddle points lead naturally to  $\langle TrP \rangle \neq \langle TrP^\dagger \rangle$ , a result that is much more difficult to obtain when fields are restricted to the real axis. The nature of these saddle points are restricted by  $\mathcal{CK}$  symmetry. The case of a single dominant saddle point is particularly tractable in theoretical analysis. In the class of models we have examined, the saddle point is not far from the real axis, as indicated by the small values of  $\psi$  and corresponding small differences between  $\langle TrP \rangle$  and  $\langle TrP^\dagger \rangle$ . This is good news for lattice simulation efforts, as it suggests only a modest excursion into the complex plane is needed. The small value of  $\psi$  also indicates a small difference for thermodynamic quantities such as pressure and internal energy between our work and previous work on phenomenological models where only real fields were used. For all six cases studied here, the maximum value of  $\psi$  occurs in the region where quark degrees of freedom are “turning on,” as indicated by crossover or critical behavior. In our previous work on Model A for massless quarks [11], we were able to show analytically how  $\psi \neq 0$  can arise from the interplay of confinement and deconfinement when  $\mu \neq 0$ , and our results here are consistent. For the two PNJL models, it is striking that the largest values of  $\psi$  occur near the critical end point. These predictions can be checked in lattice simulations by the direct measurement of  $\langle TrP \rangle$  and  $\langle TrP^\dagger \rangle$  once sufficiently effective simulation algorithms are developed.

In all six cases studied,  $\psi \neq 0$  leads to two different eigenvalues for the  $A_4$  mass matrix. In five of the six cases studied, a disorder line is found. This disorder line marks the boundary of the region where the real parts of the mass matrix eigenvalues become degenerate as the eigenvalues form a complex conjugate pair. In the PNJL models, the disorder line is closely associated with the critical line. Inside the region bounded by the disorder line, the complex conjugate pairs gives rise to color charge density oscillations. Patel has developed a scenario in which such oscillations might be observed experimentally [39, 40]. Our results indicate that the oscillations may have too large a wavelength to be directly observable in experiment, although estimates based on phenomenological models should be applied cautiously. The mass matrix eigenvalues are in principle accessible in lattice simulations via the measurement of Polyakov loop correlation functions. A direct determination of  $\kappa_I$  may

be difficult, but the disorder line itself could be determined from the merging of the values of  $Re(\kappa_1)$  with  $Re(\kappa_2)$ .

While the behavior of  $\langle TrP \rangle$ ,  $\langle TrP^\dagger \rangle$  and  $\langle \bar{\psi}\psi \rangle$ , as determined by lattice simulations, do not strongly differentiate between the two confining potential terms, Model A and Model B, the corresponding two-point correlation functions do. The most physically relevant case of PNJL models show both common features as well as clear differences in the behavior of the disorder line between Model A and Model B. In both cases, the maximum value of  $\kappa_I$  occurs slightly above and to the left of the critical end point in the  $\mu - T$  plane, in the vicinity of the region where the ratio  $Tr_F P^\dagger / Tr_F P$  is largest. In Model A, the critical line is contained within the boundary of the disorder line, but in Model B the disorder line appears to come out of the critical end point as a continuation of the critical line, a common behavior for disorder lines. Furthermore, in Model A the disorder line continues diagonally in the  $\mu - T$  plane for large  $\mu$  and  $T$ , but for Model B, the line bends over into the critical line. With Model A there is thus a possibility that the effects of the disorder line might be visible in the results of the Compressed Baryonic Matter (CBM) experiment at FAIR. The disorder line also strongly differentiates between Model A and Model B in the case of heavy quarks, so lattice simulations of either light or heavy quarks that can locate the disorder line have the potential to discriminate between the two models.

## Acknowledgments

We thank Zohar Nussinov for helpful discussions on disorder lines in condensed matter physics.

- 
- [1] Philippe de Forcrand. Simulating QCD at finite density. *PoS*, LAT2009:010, 2009.
  - [2] Sourendu Gupta. QCD at finite density. *PoS*, LATTICE2010:007, 2010.
  - [3] Gert Aarts. Complex Langevin dynamics and other approaches at finite chemical potential. *PoS*, LATTICE2012:017, 2012.
  - [4] Marco Cristoforetti, Luigi Scorzato, and Francesco Di Renzo. The sign problem and the Lefschetz thimble. *J.Phys.Conf.Ser.*, 432:012025, 2013.

- [5] H. Fujii, D. Honda, M. Kato, Y. Kikukawa, S. Komatsu, et al. Hybrid Monte Carlo on Lefschetz thimbles - A study of the residual sign problem. *JHEP*, 1310:147, 2013.
- [6] M. Cristoforetti, F. Di Renzo, A. Mukherjee, and L. Scorzato. Quantum field theories on the Lefschetz thimble. *PoS, LATTICE2013*:197, 2014.
- [7] Marco Cristoforetti, Francesco Di Renzo, Abhishek Mukherjee, and Luigi Scorzato. Monte Carlo simulations on the Lefschetz thimble: Taming the sign problem. *Phys.Rev.*, D88(5):051501, 2013.
- [8] M. Cristoforetti, F. Di Renzo, G. Erucci, A. Mukherjee, C. Schmidt, et al. An efficient method to compute the residual phase on a Lefschetz thimble. *Phys.Rev.*, D89:114505, 2014.
- [9] M. Cristoforetti, F. Di Renzo, A. Mukherjee, and L. Scorzato. Lefschetz thimbles and sign problem: First results in 0 and 4 dimensional field theories. *PoS, QCD-TNT-III*:010, 2014.
- [10] Denes Sexty. New algorithms for finite density QCD. 2014.
- [11] Hiromichi Nishimura, Michael C. Ogilvie, and Kamal Pangaeni. Complex saddle points in QCD at finite temperature and density. *Phys.Rev.*, D90:045039, 2014.
- [12] Peter N. Meisinger, Travis R. Miller, and Michael C. Ogilvie. Phenomenological equations of state for the quark gluon plasma. *Phys.Rev.*, D65:034009, 2002.
- [13] Gert Aarts and Ion-Olimpiu Stamatescu. Stochastic quantization at finite chemical potential. *JHEP*, 0809:018, 2008.
- [14] Carl M. Bender and Stefan Boettcher. Real spectra in nonHermitian Hamiltonians having PT symmetry. *Phys.Rev.Lett.*, 80:5243–5246, 1998.
- [15] Peter N. Meisinger and Michael C. Ogilvie. PT Symmetry in Classical and Quantum Statistical Mechanics. *Phil.Trans.Roy.Soc.Lond.*, A371:20120058, 2013.
- [16] Simon Hands, Timothy J. Hollowood, and Joyce C. Myers. Numerical Study of the Two Color Atworld. *JHEP*, 1012:057, 2010.
- [17] Simon Hands, Timothy J. Hollowood, and Joyce C. Myers. QCD with Chemical Potential in a Small Hyperspherical Box. *JHEP*, 1007:086, 2010.
- [18] Timothy J. Hollowood, S. Prem Kumar, and Joyce C. Myers. Weak coupling large-N transitions at finite baryon density. *JHEP*, 1111:138, 2011.
- [19] Timothy J. Hollowood and Joyce C. Myers. Deconfinement transitions of large N QCD with chemical potential at weak and strong coupling. *JHEP*, 1210:067, 2012.
- [20] Kenji Fukushima. Chiral effective model with the Polyakov loop. *Phys.Lett.*, B591:277–284,

- 2004.
- [21] Joyce C. Myers and Michael C. Ogilvie. New phases of  $SU(3)$  and  $SU(4)$  at finite temperature. *Phys.Rev.*, D77:125030, 2008.
  - [22] Mithat Unsal. Abelian duality, confinement, and chiral symmetry breaking in  $QCD(adj)$ . *Phys.Rev.Lett.*, 100:032005, 2008.
  - [23] Michael Buballa and Igor A. Shovkovy. A Note on color neutrality in NJL-type models. *Phys.Rev.*, D72:097501, 2005.
  - [24] John Stephenson. Ising model with antiferromagnetic next-nearest-neighbor coupling: Spin correlations and disorder points. *Phys. Rev. B*, 1:4405–4409, Jun 1970.
  - [25] John Stephenson. Two one-dimensional ising models with disorder points. *Canadian Journal of Physics*, 48(14):1724–1734, 1970.
  - [26] Walter Selke. The annni model âa theoretical analysis and experimental application. *Physics Reports*, 170(4):213 – 264, 1988.
  - [27] C.P. Korthals Altes, Robert D. Pisarski, and Annamaria Sinkovics. The Potential for the phase of the Wilson line at nonzero quark density. *Phys.Rev.*, D61:056007, 2000.
  - [28] Mithat Unsal and Laurence G. Yaffe. Center-stabilized Yang-Mills theory: Confinement and large  $N$  volume independence. *Phys.Rev.*, D78:065035, 2008.
  - [29] Michael C. Ogilvie. Phases of Gauge Theories. *J.Phys.*, A45:483001, 2012.
  - [30] S.P. Klevansky. The Nambu-Jona-Lasinio model of quantum chromodynamics. *Rev.Mod.Phys.*, 64:649–708, 1992.
  - [31] Hiromichi Nishimura and Michael C. Ogilvie. A PNJL Model for Adjoint Fermions with Periodic Boundary Conditions. *Phys.Rev.*, D81:014018, 2010.
  - [32] Tetsuo Hatsuda and Teiji Kunihiro. QCD phenomenology based on a chiral effective Lagrangian. *Phys.Rept.*, 247:221–367, 1994.
  - [33] Tohru Eguchi. A New Approach to Collective Phenomena in Superconductivity Models. *Phys.Rev.*, D14:2755, 1976.
  - [34] Shotaro Imai, Hiroshi Toki, and Wolfram Weise. Quark-Hadron Matter at Finite Temperature and Density in a Two-Color PNJL model. *Nucl.Phys.*, A913:71–102, 2013.
  - [35] Thomas C. Blum, James E. Hetrick, and Doug Toussaint. High density QCD with static quarks. *Phys.Rev.Lett.*, 76:1019–1022, 1996.
  - [36] Kouji Kashiwa, Robert D. Pisarski, and Vladimir V. Skokov. Critical endpoint for deconfine-



- ment in matrix and other effective models. *Phys.Rev.*, D85:114029, 2012.
- [37] Peter N. Meisinger and Michael C. Ogilvie. Complete high temperature expansions for one loop finite temperature effects. *Phys.Rev.*, D65:056013, 2002.
- [38] Bernd-Jochen Schaefer, Jan M. Pawłowski, and Jochen Wambach. The Phase Structure of the Polyakov–Quark-Meson Model. *Phys.Rev.*, D76:074023, 2007.
- [39] Apoorva Patel. Flux Tube Model Signals for Baryon Correlations in Heavy Ion Collisions. *Phys.Rev.*, D85:114019, 2012.
- [40] Apoorva Patel. Baryon Number Correlations in Heavy Ion Collisions. *PoS*, LATTICE2012:096, 2012.